Chemical Physics Letters 731 (2019) 136606

Contents lists available at ScienceDirect

Chemical Physics Letters

journal homepage: www.elsevier.com/locate/cplett

Research paper

Electric field tuning of dynamical dielectric function in phosphorene

Khang D. Pham[a,b], Nguyen N. Hieu[c], Masoumeh Davoudiniya[d], Le T.T. Phuong[e,*], Bui D. Hoi[e,1], Chuong V. Nguyen[f], Huynh V. Phuc[g], Pham T.C. Van[h], Tran C. Phong[i]

[a] Laboratory of Applied Physics, Advanced Institute of Materials Science, Ton Duc Thang University, Ho Chi Minh City, Viet Nam
[b] Faculty of Applied Sciences, Ton Duc Thang University, Ho Chi Minh City, Viet Nam
[c] Institute of Research and Development, Duy Tan University, Da Nang, Viet Nam
[d] Department of Energy Engineering and Physics, Amirkabir University of Technology, 14588 Tehran, Iran
[e] Department of Physics, University of Education, Hue University, Hue, Viet Nam
[f] Department of Materials Science and Engineering, Le Quy Don Technical University, Ha Noi, Viet Nam
[g] Division of Theoretical Physics, Dong Thap University, Dong Thap 870000, Viet Nam
[h] Department of Physics, Thua Thien Hue College of Education, Thua Thien Hue, Viet Nam
[i] The Vietnam National Institute of Educational Sciences, Hanoi, Viet Nam

HIGHLIGHTS

- Anisotropic electro-optical properties of monolayer black phosphorus in the presence electric field effects are investigated.
- For the frequencies beneath the band gap, the refraction (absorption) along the armchair direction of phosphorene is smaller (larger) than the zigzag direction.
- For the frequencies above the band gap, the dynamical dielectric function decreases with the electric field independent of the direction.

ABSTRACT

We present electric field effects on the optical field-dependent dielectric function of phosphorene. We use a two-band model and the Kubo formula to obtain refractive index and absorption coefficient. From our findings, the refraction (absorption) along the armchair direction is smaller (larger) than the zigzag direction for the optical energies close to and larger than the band gap. Moreover, we find that for frequencies beneath the band gap, dynamical dielectric function decreases with the electric field independent of the orientation, whereas there is a strong anisotropic treatment above the band gap.

1. Introduction

Developing two-dimensional (2D) materials for the opto-nanoelectronics are extensively studied lately. Due to the unsuitability of gapless graphene [1–3] in the semiconductor industry, other 2D gapped materials based on the molybdenum, silicon, boron, and phosphorus atoms have been synthesized [4–10] quickly, confirming that the family of 2D materials is growing fast. Among 2D materials, the black phosphorus introduces remarkable electro-optical properties [11–13]. The key feature in this puckered 2D system is related to its strong anisotropic property [14,15], which leads to the orientation-dependent carrier effective mass and velocity in contrast to other 2D gapped systems.

The unique properties of phosphorene originating from this anisotropy result in a high ON/OFF current ratio [16,17], high carrier mobility [18], a mechanical malleability [19], the anisotropic thermal and electrical conductivity [20]. Due to these features, phosphorene is more applicable compared to other materials in electronic [11,21] and thermoelectric devices [20,22]. On the other hand, many works have shown that the semiconductor nature of phosphorene can be tuned through different methods such as doping [23,24], defect [25], hydrogenation [26–29], strain and electric field [30–34].

Giant Stark effect stemming from the external electric field (gate voltage) is an important effect which comes into play role in tuning the electronic phase of phosphorene [35–37]. Thereby, studying the electric-field-dependent optical properties of phosphorene is interesting. However, in order to improve and solve the shortcomings of 2D semiconductor industry, investigation of electric field-dependent refraction and absorption processes of phosphorene subjected to an optical field is important. To the best of our knowledge, this open issue has not been theoretically addressed yet, which is the main aim of the present paper.

* Corresponding author.
E-mail addresses: phamdinhkhang@tdtu.edu.vn (K.D. Pham), davoudiniya.m@aut.ac.ir (M. Davoudiniya), thuphuonghueuni@gmail.com (L.T.T. Phuong), buidinhhoi@hueuni.edu.vn (B.D. Hoi).
[1] Co-corresponding author.

https://doi.org/10.1016/j.cplett.2019.136606
Received 10 June 2019; Received in revised form 12 July 2019; Accepted 12 July 2019
Available online 15 July 2019

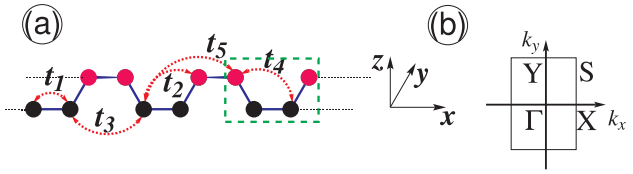

Fig. 1. (a) Side view of monolayer phosphorene. The armchair and zigzag direction are along the x and y axis, respectively. The electric field is applied along the z axis. The unit cell of monolayer phosphorene consisting of four phosphorus atoms is shown by a dashed rectangle in (a). The first Brillouin zone of phosphorene is depicted in (b) for which $-\pi/a \leqslant k_x \leqslant +\pi/a$ and $-\pi/b \leqslant k_y \leqslant +\pi/b$ where $a = 4.42936$ Å and $b = 3.27$ Å is the length of the unit cell along the armchair and zigzag direction, respectively.

In this paper, we show the electric field effects on the band gap and the dynamical dielectric function in phosphorene. These findings provide new physical insights, making a better understanding of the optical responses of phosphorene. To this end, we use a two-band tight-binding model and employ the Kubo formalism implemented in the linear response theory to obtain the optical conductivity and eventually the dynamical dielectric function. Finally, the refraction and absorption coefficients are calculated in the presence of an external electric field at different optical frequencies.

The paper is organized as follows. In Section 2 the two-band Hamiltonian model is reviewed. Section 3 presents briefly the Kubo formula and the dynamical dielectric function. In Section 4, we analyze the numerical results and finally in Section 5 we end the paper by remarking the main findings.

2. Theoretical model

Since the crystal structure of phosphorene consists of two sublayers with four the same atoms per sublayer, as shown in Fig. 1(a), the electric field-induced tight-binding Hamiltonian matrix of phosphorene for one p_z orbital in the reciprocal space reads [38,39]

$$\mathcal{H}_{\vec{k}} = \begin{pmatrix} h^{11}_{\vec{k}} + V/2 & h^{12}_{\vec{k}} \\ h^{12,*}_{\vec{k}} & h^{11}_{\vec{k}} - V/2 \end{pmatrix}, \tag{1}$$

where the momenta $\vec{k}$ belong to the first Brillouin zone (FBZ) of phosphorene. On the other hand, using the symmetry between two sublayers, the momenta-dependent elements, so-called the structure factors, are calculated as $h^{11}_{\vec{k}} = 4t_4\cos(k_x a/2)\cos(k_y b/2)$ and $h^{12}_{\vec{k}} = 2t_1 e^{-ik_x a_{1x}}\cos(k_y b/2) + t_2 e^{ik_x a_{2x}} + 2t_3 e^{ik_x a_{3x}}\cos(k_y b/2) + t_5 e^{-ik_x a_{5x}}$. Note that only five nearest neighbor lattice sites are considered with the hopping integral energies $t_1 = -1.220$ eV, $t_2 = +3.665$ eV, $t_3 = -0.205$ eV, $t_4 = -0.105$ eV, and $t_5 = -0.055$ eV [38,40] [see Fig. 1(a)]. V stands for the applied gate voltage on the top ($+V/2$) and bottom ($-V/2$) of sublayers [41,42]. The distance between the intra- and inter-planar nearest-neighbor atoms projected to the x direction are given by $a_{1x} = 1.41763$ Å, $a_{2x} = 2.16400$ Å, $a_{3x} = 3.01227$ Å, $a_{4x} = 2.21468$ Å, and $a_{5x} = 3.63258$ Å [38,40,39]. Diagonalizing the Hamiltonian above, the eigenvalues read

$$\mathcal{E}_{\vec{k},\nu} = h^{11}_{\vec{k}} + \nu\sqrt{\frac{V^2}{4} + h^{12}_{\vec{k}} h^{12,*}_{\vec{k}}}, \tag{2}$$

where $\nu = +1$ and $\nu = -1$ refers to the conduction band and valence band, respectively.

Using the dispersion energy obtained above, one is able to characterize the electronic phase of monolayer phosphorene, i.e. semiconducting phase. The shadowed area in Fig. 2 shows a band gap of about $\mathcal{E}_g = 1.52$ eV for monolayer phosphorene [38], which increases with the gate voltage V, in agreement with Refs. [38,43]. The curves show that the direct band gap of the system keeps its nature at all electric fields and there is no direct-to-indirect phase transition. A key

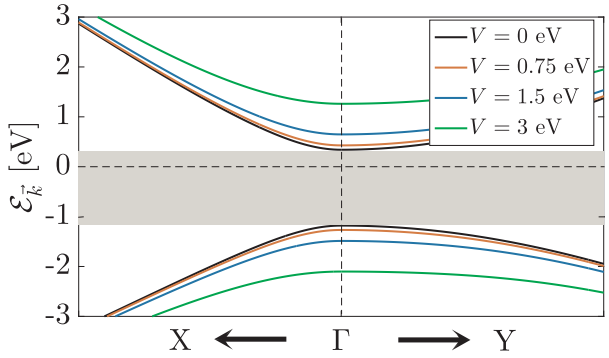

Fig. 2. The variation of the electronic band structure of monolayer phosphorene with the electric field V. The direct band gap increases with V.

role of strong anisotropic properties of phosphorene originates from this band structure for which the bands along the armchair (X ← Γ) and zigzag (Γ→Y) direction are not the same. These lead to the orientation-dependent electro-optical properties. Let us focus on the main aim of the paper, i.e. the electric field effects on the dynamical dielectric function of phosphorene.

3. Dynamical dielectric function

To calculate the dynamical dielectric function of phosphorene, we consider an effective finite thickness of $d \simeq 1$ nm [44] as well as the static relative permittivity of the system $\varepsilon_r \simeq 5.76$[44]. Using these parameters and also the permittivity in vacuum ε_0, the dynamical dielectric function ε reads [45,46]

$$\varepsilon_{\beta\beta}(\omega) = \varepsilon_r + \mathrm{i}\frac{\sigma^{\mathrm{inter}}_{\beta\beta}(\omega)}{\varepsilon_0 \omega d}. \tag{3}$$

in which $\sigma^{\mathrm{inter}}_{\beta\beta}(\omega)$ for $\beta \in \{x, y\}$ are the diagonal terms of the interband optical conductivity tensor and ω is the incident optical frequency. In the equation above, interband optical conductivity components are calculated using the Kubo formula within the linear response theory [39,47–49]

$$\frac{\sigma^{\mathrm{inter}}_{\beta\beta}(\omega)}{\sigma_0} = -\frac{4\mathrm{i}}{\hbar\omega}\sum_{\vec{k}\in\mathrm{FBZ}} (\chi^{\beta}_{\vec{k}})^2 \cdot \frac{(n^{\mathrm{FD}}_{\vec{k},+} - n^{\mathrm{FD}}_{\vec{k},-})(\mathcal{E}_{\vec{k},+} - \mathcal{E}_{\vec{k},-})}{(\hbar\omega + \mathrm{i}\eta)^2 - (\mathcal{E}_{\vec{k},+} - \mathcal{E}_{\vec{k},-})^2}. \tag{4}$$

where $\sigma_0 = e^2/\hbar$ is the universal value for the optical conductivity. The finite damping between the valence and conduction bands is given by $\eta = 10$ meV and $n^{\mathrm{FD}}_{\vec{k},\pm} = 1/1 + exp[(\mathcal{E}_{\vec{k},\pm} - \mu)/k_B T]$ stands for the Fermi–Dirac distribution function at the chemical potential μ and temperature T (k_B being the Boltzmann constant). Also, $\chi^{\beta}_{\vec{k}}$ refers to the direction-dependent velocity of carriers in phosphorene [38,40,43,39], given by

$$\begin{aligned}\chi^{x}_{\vec{k}} &= -2t_1 a_{1x}\cos(k_y b/2)\cos(k_x a_{1x} + \theta_{\vec{k}}) \\ &+ t_2 a_{2x}\cos(k_x a_{2x} - \theta_{\vec{k}}) \\ &+ 2t_3 a_{3x}\cos(k_y b/2)\cos(k_x a_{3x} - \theta_{\vec{k}}) \\ &- t_5 a_{5x}\cos(k_x a_{5x} + \theta_{\vec{k}}),\end{aligned} \tag{5a}$$

$$\begin{aligned}\chi^{y}_{\vec{k}} &= +bt_1\sin(k_y b/2)\sin(k_x a_{1x} + \theta_{\vec{k}}) \\ &- bt_3\sin(k_y b/2)\sin(k_x a_{3x} - \theta_{\vec{k}}).\end{aligned} \tag{5b}$$

where $e^{\mathrm{i}\theta_{\vec{k}}} = \sqrt{h^{12}_{\vec{k}}/h^{12,*}_{\vec{k}}}$.

From Eq. (4), it is clear that the interband optical conductivity possesses a real and an imaginary part, thus, the dynamical dielectric function, given by Eq. (3) can be rewritten as

$$\varepsilon_{\beta\beta}(\omega) = \varepsilon_1^{\beta\beta}(\omega) + i\varepsilon_2^{\beta\beta}(\omega). \tag{6}$$

with

$$\varepsilon_1^{\beta\beta}(\omega) = \varepsilon_r - \frac{\mathrm{Im}[\sigma_{\beta\beta}^{\mathrm{inter}}(\omega)/\sigma_0]}{\varepsilon_0\omega d}, \tag{7a}$$

$$\varepsilon_2^{\beta\beta}(\omega) = \frac{\mathrm{Re}[\sigma_{\beta\beta}^{\mathrm{inter}}(\omega)/\sigma_0]}{\varepsilon_0\omega d}. \tag{7b}$$

This relation leads to a complex refractive index $\sqrt{\varepsilon_{\beta\beta}(\omega)} = n_{\beta\beta}(\omega) + i\kappa_{\beta\beta}(\omega)$ for which [50]

$$n_{\beta\beta}(\omega) = \sqrt{\frac{\sqrt{|\varepsilon_{\beta\beta}(\omega)|} + \varepsilon_1^{\beta\beta}(\omega)}{2}}, \tag{8a}$$

$$\kappa_{\beta\beta}(\omega) = \sqrt{\frac{\sqrt{|\varepsilon_{\beta\beta}(\omega)|} - \varepsilon_1^{\beta\beta}(\omega)}{2}}. \tag{8b}$$

where $\kappa_{\beta\beta}(\omega)$ is the extinction coefficient, while the parameter $n_{\beta\beta}(\omega)$ determines the refraction rate of the system when it is subjected to an optical field with frequency ω. Although $\kappa_{\beta\beta}(\omega)$ itself can be calculated and studied, however, the most related important quantity to $\kappa_{\beta\beta}(\omega)$ is absorption coefficient $\alpha_{\beta\beta}(\omega) = 2\omega\kappa_{\beta\beta}(\omega)/c$ in which c is the velocity of light.

4. Numerical results and discussion

The dynamical dielectric function $\varepsilon(\omega)$ tells us that the refraction and absorption of the phosphorene in the presence of an external perpendicular electric field depend strongly on the interband optical conductivity of the system. On the other hand, from Eq. (4), the interband optical conductivity connects to the electronic dispersion energies $\mathcal{E}_{\vec{k},\nu}$. Thereby, obviously, the $\varepsilon(\omega)$ quantity must not be the same along the armchair and zigzag directions. In this section, we focus on the orientation- and electric field-dependent dynamical dielectric function in order to see how the system responses to an optical field in the presence of an applied gate voltage on the top and bottom of sublayers in phosphorene.

Note that the methodology must not deal with unrealistic parameter ranges, for this reason, the selected range for the electric field is from 0 to 3 eV. This allows the experimentalists to catch the results as well. As for the temperature parameter, which comes into play role in Eq. (4), we stress that the thermal energy $k_B T$ at room temperature is around 26 meV while the band gap of monolayer phosphorene is around 1.5 eV. From this huge difference, we omit the temperature effects in the present paper and we have fixed the temperature throughout the paper at 10 K. As the last point, for the sake of convenience, we divide the optical frequencies into three beneath, near and above the band gap regimes, i.e. $\hbar\omega < \mathcal{E}_g$, $\hbar\omega \simeq \mathcal{E}_g$ and $\hbar\omega > \mathcal{E}_g$. Additionally, we have studied the high enough optical frequency case as well in order to study the validity of our model.

Before interpreting the results, we would like to point out a very important and expected finding in our plots. Around the Γ point of the electronic band structure, see Fig. 2, the carrier effective mass, originating from the curvature of bands, along the armchair ($X \leftarrow \Gamma$) direction is smaller than the zigzag ($\Gamma \rightarrow Y$) one, whereas the carrier velocity is larger. This clarifies that the interband optical conductivity along the armchair direction must be larger than the zigzag one. Thereby, for the case of $\hbar\omega \simeq \mathcal{E}_g$, we expect a smaller refractive index $n(\omega)$ but a larger absorption coefficient $\alpha(\omega)$ along the armchair direction, as confirmed nicely in panels (b) and (f) of Figs. 3 and 4 (blue[2] curves).

In general, the path of entered incident light into a material is tracked by the dimensionless number $n(\omega)$, which describes the refraction index of the system when touching the incident light with frequency ω. Theory of relativity expresses that this number must be below the unity, as confirmed in our numerical calculations. Obviously,

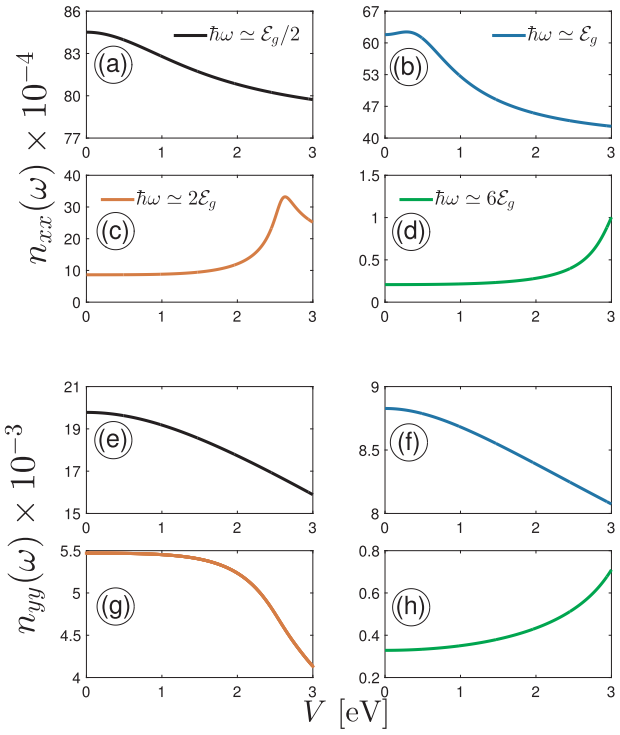

Fig. 3. The real part of dynamical dielectric function, refractive index, as a function of the potential V for four different optical energies $\hbar\omega \simeq \mathcal{E}_g/2$, $\hbar\omega \simeq \mathcal{E}_g$, $\hbar\omega \simeq 2\mathcal{E}_g$, and $\hbar\omega \simeq 6\mathcal{E}_g$ along the {(a)–(d)} armchair direction and {(e)–(h)} zigzag direction. The temperature is fixed at $T = 10$ K in these plots.

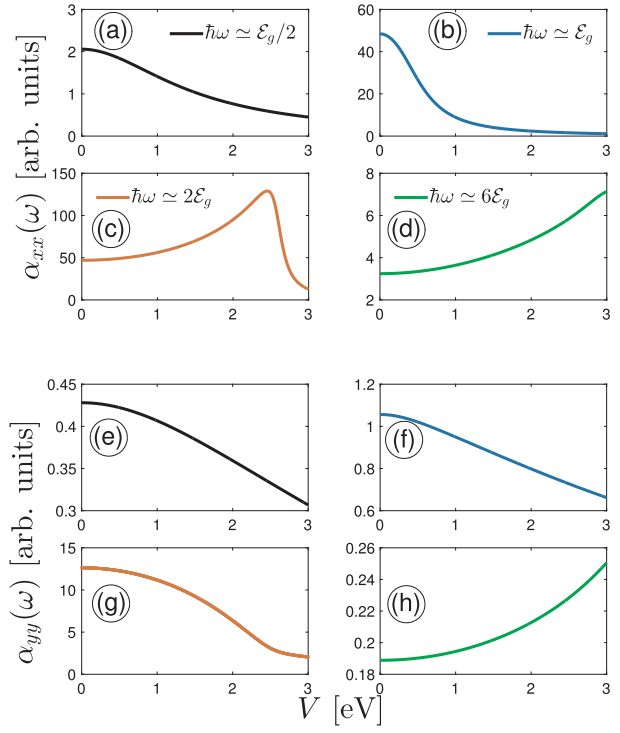

Fig. 4. The same as Fig. 3 but for the modified imaginary part of the dynamical dielectric function, i.e. absorption coefficient.

[2] For interpretation of color in Figs. 3 and 4, the reader is referred to the web version of this article.

the incident light after crossing the interface moves into the phosphorene and propagates with the same frequency ω but a shorter wavelength. This wavelength can be extremely controlled by the electric field because Fig. 2 shows clearly that the wave vectors of carriers strongly depend on the electric field strength. For this reason, the coupling between the carrier wave vector and the light wave vector is influenced by the electric field.

Fig. 3 illustrates the frequency- and electric field-dependent refractive index at temperature $T = 10$ K. In the case of $\hbar\omega \simeq \mathcal{E}_g/2$, the refractive index decreases with the gate voltage for both directions (panels (a) and (e)) and the order of magnitude along the armchair direction is much smaller than the zigzag one, as expected. As soon as the optical energy is increased, the intensity of $n(\omega)$ decreases. For the case of $\hbar\omega \simeq \mathcal{E}_g$, the decreasing trend with the electric field is still valid. The difference between results along the armchair and zigzag direction in this regime refers to the *exponential decay* of the curve along the armchair direction (Fig. 3(b)), whereas an almost linear behavior can be seen along the zigzag one (Fig. 3(f)). However, the key difference between the armchair and zigzag directions comes from the optical frequencies above the band gap, but not strong ones. Fig. 3(c) and (g) (red curves) reveal that in the case of $\hbar\omega \simeq 2\mathcal{E}_g$, the refractive index along the armchair edge increases with V and reaches a maximum at $V \simeq 2.75$ eV, while along the zigzag edge, the number $n(\omega)$ does not change up to $V \simeq 1$ eV and then decreases rapidly. This is the main point of our results, which signalizes the inherent strong anisotropic property of phosphorene manifesting itself in the refraction coefficient corresponding to the frequencies above the band gap of the system.

Let us investigate the higher optical frequencies as well. Panels (d) and (h) in Fig. 3 represent the case of $\hbar\omega \simeq 6\mathcal{E}_g$ for which our model does not contain any bands and the isotropic curves are expected for the optical conductivities and eventually dynamical dielectric function. Both directions possess an increasing treatment with V with a slight difference between the amounts of $n(\omega)$. Of course, one can consider another band model with more bands to include more information at high enough frequencies, however; this is outside of the scope of the present work.

Now we turn to the optical absorption behavior as a function of optical frequency and the electric field in Fig. 4. Generally, the penetration of an incident light into a material before complete absorption is shown by the $\alpha(\omega)$ quantity. In other words, the transmission of the light from a material is measured by this coefficient. Of course, the optical frequency here is much more than important. Fig. 4(a) and (e) show that the absorption coefficient independent of the orientation decreases with the electric field when the optical energy is less than the band gap. Again, an exponential decay (a decreasing behavior) for x (y)-absorption with V is achieved for the case of $\hbar\omega \simeq \mathcal{E}_g$, as presented in Fig. 4(b) and (f). Similar to the case of refractive index, there is a critical electric field strength ($V \simeq 2.5$ eV) at which the absorption spectra is maximized along the armchair edge, whereas there is no critical electric field for the zigzag edge and $\alpha_{yy}(\omega)$ decreases with V gradually, see Fig. 4(c) and (g). When exciting the carriers from the valence band to the conduction band with the optical frequencies much higher than the band gap size, weak absorptions like the lower frequencies emerge, see Fig. 4(d) and (h). These weak absorptions increase with the electric field slightly.

5. Conclusions

In summary, we have theoretically studied the dynamical dielectric function of monolayer phosphorene under a perpendicular electric field. In particular, the photon energy- and electric field-dependent refractive index and absorption coefficient are investigated using an effective Hamiltonian model and the Kubo formalism. After addressing the increase of the band gap with the electric field, we have shown that these optical responses are strongly anisotropic and influenced by the electric field along the armchair and zigzag directions, as expected. We have found that while there is a strong anisotropic trend in both refraction and absorption phenomena with the electric field for the frequencies above the band gap, they behave the same for the optical energies beneath and near the band gap. These findings validate phosphorene as a promising alternative to other 2D materials in optoelectronics.

Declaration of Competing Interest

None.

Acknowledgements

This research is funded by Vietnam National Foundation for Science and Technology Development (NAFOSTED) under grant number 103.01-2017.361.

Appendix A. Supplementary material

Supplementary data associated with this article can be found, in the online version, at https://doi.org/10.1016/j.cplett.2019.136606.

References

[1] A.H. Castro Neto, F. Guinea, N.M.R. Peres, K.S. Novoselov, A.K. Geim, Rev Mod. Phys. 81 (2009) 109.
[2] K. Novoselov, et al., Nature 438 (2005) 197.
[3] M. Yarmohammadi, Phys. Rev. B 98 (15) (2018) 155424.
[4] Z. Lin, et al., 2D Mater. 3 (2016) 022002.
[5] Z. Tian, C. Guo, M. Zhao, R. Li, J. Xue, ACS Nano 11 (2) (2017) 2219.
[6] L. Tao, et al., Nat. Nanotechnol. 10 (2015) 227.
[7] B.D. Hoi, M. Yarmohammadi, J. Magn. Magn. Mater. 451 (2018) 57.
[8] M. Yarmohammadi, Phys. Lett. A 381 (2017) 1261.
[9] M. Yarmohammadi, Solid State Commun. 253 (2017) 57.
[10] H.D. Bui, M. Yarmohammadi, Solid State Commun. 280 (2018) 39.
[11] J. Dai, X.C.J. Zeng, Phys. Chem. Lett. 5 (2014) 1289.
[12] Y. Cai, G. Zhang, Y. Zhang, Sci. Rep. 4 (2014) 6677.
[13] W. Lu, et al., Nano Res. 7 (6) (2014) 853.
[14] N. Mao, et al., J. Am. Chem. Soc. 138 (2015) 300.
[15] D. Cakir, C. Sevik, F.M. Peeters, Phys. Rev. B 92 (2015) 165406.
[16] B. Radisavljevic, A. Radenovic, J. Brivio, V. Giacometti, A. Kis, Nat. Nanotechnol. 6 (2011) 147.
[17] S.P. Koenig, R.A. Doganov, H. Schmidt, A.H. Catro Neto, B. özyilmaz, Appl. Phys. Lett. 104 (2014) 103106.
[18] K.F. Mak, C. Lee, J. Hone, J. Shan, T.F. Heinz, Phys. Rev. Lett. 105 (2010) 136805.
[19] Q. Wei, X. Peng, Appl. Phys. Lett. 104 (2014) 251915.
[20] R. Fei, A. Faghaninia, R. Soklaski, J.A. Yan, C. Lo, L. Yang, Nano Lett. 14 (2014) 6393.
[21] M. Buscema, D.J. Groenendijk, G.A. Steele, H.S.J. van der Zant, A. Castellanos-Gomez, Nat. Commun. 5 (2014) 4651.
[22] S.-Y. Ma, L.-M. Liu, S.-Q. Wang, J. Mater. Sci. 49 (2014) 737.
[23] M. Yarmohammadi, Phys. Lett. A 380 (48) (2016) 4062.
[24] H.D. Bui, L.T.T. Phuong, M. Yarmohammadi, EPL 124 (2) (2018) 27001.
[25] G. Wang, R. Pandey, S.P. Karna, Appl. Phys. Lett. 106 (2015) 173104.
[26] J. He, K.-Q. Chen, Z.-Q. Fan, L.-M. Tang, W.P. Hu, Appl. Phys. Lett. 97 (2010) 193305.
[27] J. Zeng, K.-Q. Chen, J. He, X.-J. Zhang, C.Q. Sun, J. Phys. Chem. C 115 (2011) 25072.
[28] S.-Z. Chen, F. Xie, F. Ning, Y.-Y. Liu, W.-X. Zhou, J.-F. Yu, K.-Q. Chen, Carbon 111 (2017) 867.
[29] B.D. Hoi, M. Yarmohammadi, Phys. Lett. A 382 (2018) 3298.
[30] H. Guo, N. Lu, J. Dai, X. Wu, X.C. Zeng, J. Phys. Chem. C 118 (2014) 14051.
[31] S. Appalakondaiah, G. Vaitheeswaran, S. Lebegue, N.E. Christensen, A. Svane, Phys. Rev. B 86 (2012) 035105.
[32] N.D. Hien, M. Davoudiniya, K. Mirabbaszadeh, L.T.T. Phuong, M. Yarmohammadi, Chem. Phys. 522 (2019) 249.
[33] H.D. Bui, M. Yarmohammadi, Physica E 103 (2018) 76.
[34] P.T.T. Le, M. Davoudiniya, K. Mirabbaszadeh, B.D. Hoi, M. Yarmohammadi, Physica E 106 (2019) 250.
[35] L. Kou, C. Li, Z. Zhang, W. Guo, J. Phys. Chem. C 114 (2010) 1326.
[36] Q. Yue, S. Chang, J. Kang, X. Zhang, Z. Shao, S. Qin, J. Li, J. Phys. Condens. Matter 24 (2012) 335501.
[37] K. Dolui, C.D. Pemmaraju, S. Sanvito, ACS Nano 6 (2012) 4823.
[38] S. Yuan, A.N. Rudenko, M.I. Katsnelson, Phys. Rev. B 91 (2015) 115436.
[39] C.H. Yang, J.Y. Zhang, G.X. Wang, C. Zhang, Phys. Rev. B 97 (2018) 245408.
[40] A.N. Rudenko, M.I. Katsnelson, Phys. Rev. B 89 (2014) 201408(R).
[41] H. Gui-Qin, X. Zhong-Wen, Chin. Phys. B 25 (2) (2016) 027402.
[42] D.J.P. de Sousa, L.V. de Castro, D.R. da Costa, J. Milton Pereira Jr., T. Low, Phys.

Rev. B 96 (2017) 155427.
[43] M. Ezawa, New J. Phys. 16 (2014) 115004.
[44] Z. Liu, K. Aydin, Nano Lett. 16 (2016) 3457.
[45] C.H. Yang, Q.F. Li, Y.Y. Chen, W. Fu, Physica E 112 (2019) 1.
[46] G. Mahan, Many Particle Physics, Plenum Press, New York, 1993.
[47] R. Kubo, J. Phys. Soc. Japan 12 (1957) 570.
[48] D.Q. Khoa, M. Davoudiniya, B.D. Hoi, M. Yarmohammadi, RSC Adv. 9 (33) (2019) 19006.
[49] P.T.T. Le, K. Mirabbaszadeh, M. Yarmohammadi, J. Appl. Phys. 125 (19) (2019) 193101.
[50] P.T.T. Le, K. Mirabbaszadeh, M. Yarmohammadi, RSC Adv. 9 (5) (2019) 2829.